SURFACE PHYSICS AND THIN FILMS

Magnetic and Structural Properties of $Fe_{87}Pt_{13}$–Al_2O_3 Composite Thin Films Synthesized by Solid-State Reactions

V. S. Zhigalov[a], *, V. G. Myagkov[a], L. E. Bykova[a], G. N. Bondarenko[b],
A. A. Matsynin[a], and M. N. Volochaev[a,c]

[a] *Kirensky Institute of Physics, Siberian Branch, Russian Academy of Sciences,
Krasnoyarsk, 660036 Russia*
[b] *Institute of Chemistry and Chemical and Technology, Siberian Branch, Russian Academy of Sciences,
Krasnoyarsk, 660036 Russia*
[c] *Siberian State Aerospace University, Krasnoyarsk, 660014 Russia*
*e-mail: zhigalov@iph.krasn.ru
Received June 28, 2016

Abstract—The structural and magnetic properties of $Fe_{87}Pt_{13}$ films synthesized by solid-state reactions and $Fe_{87}Pt_{13}$–Al_2O_3 composite films fabricated by aluminothermy are investigated. It is shown that the synthesized samples of both types are characterized by the rotational magnetic anisotropy, when the easy magnetization axis in the film plane can be set by a magnetic field. It is established that the value of rotational magnetic anisotropy in the $Fe_{87}Pt_{13}$–Al_2O_3 composite films is higher than in the $Fe_{87}Pt_{13}$ samples by an order of magnitude. The rotational magnetic anisotropy is assumed to be caused by the exchange coupling of the $L1_0$–FePt phase with the $L1_2$–Fe_3Pt phase in the $Fe_{87}Pt_{13}$ films and magnetic iron oxides in the $Fe_{87}Pt_{13}$–Al_2O_3 samples.

1. INTRODUCTION

The $L1_0$-ordered FePd, CoPt, and FePt thin films have a tetragonal structure and are interesting for application due to their high magnetic anisotropy [1, 2]. According to the phase equilibrium diagram, the Fe–Pt system also contains the ordered $L1_2$–$FePt_3$ and $L1_2$–Fe_3Pt phases and chemically disordered fcc solid solutions (fcc-A_1). In studying the Fe_xPt_{1-x} samples, researches exert the most intensive efforts to establish the correlations between the magnetic properties and structural parameters of the synthesized $L1_0$, $L1_2$, and A_1 phases both in the thin-film [3–8] and nanostructured state [9, 10]. However, in the samples containing small (~3 nm) structural formations, the role of magnetic interactions affecting the parameters of these materials is modified. In view of this, it is necessary for application to enclose magnetic grains in insulating media. The insulating composite matrices are formed from silicon oxides or nitrides [11], aluminum oxides, or, depending on the purpose of use, normal (Cu, Cr), noble (Au, Ag), and refractory (W) metals, graphite, etc. [11–15]. The $L1_0$-ordered FePt and CoPt samples formed from small grains in an insulating matrix are chemically stable, behave superparamagnetically, and are characterized by weak magnetic interactions, high magnetic anisotropy ($K_u \sim 7 \times$

10^7 erg/cm^3), saturation magnetization ($M_s > 1150$ emu/cm^3), and coercivity ($H_c > 3$ kOe). Therefore, they can be recommended for high-density data recording or thin-film permanent magnets [16]. As was shown, e.g., in [17], the $L1_2$–Fe_3Pt films also exhibit high perpendicular magnetic anisotropy, the nature of which has been investigated. It should be taken into account that the cubic symmetry of the $L1_2$ films does not suggest the high anisotropy, including perpendicular magnetic, energies. However, the $L1_2$–Fe_3Pt composite thin films in an insulating matrix can have a large magnetic anisotropy constant, depending on the fabrication and heat treatment conditions. To study the magnetoresistance and tunneling mechanisms and develop devices on their basis, it is often necessary to fabricate granular systems with formations with the cubic $L1_2$–Fe_3Pt lattice as magnetic grains. The overwhelming majority of studies on the techniques for fabricating Fe_xPt_{1-x} composite magnetic films and their properties are aimed at investigations near the equiatomic composition, whereas there has been a lack of works devoted to the films with higher iron content.

It is well-known that all the classical types of magnetic anisotropies are described by the sinusoidal laws. However, thin films are characterized by the alterna-

tive anisotropy type—rotational magnetic anisotropy (RMA), when the easy axis tends to align in the magnetic field direction. As we showed previously [18], the epitaxial $L1_0-CoPt(111)$ thin films synthesized by the solid-state reaction of elemental Co and Pt layers have high RMA exceeding the film anisotropy [18].

In this work, we investigated the magnetic and structural properties and RMA of the $Fe_{87}Pt_{13}$ films synthesized by the solid-state reactions between the Pt(001) and Fe(001) epitaxial layers upon heat treatment [19–22]. The $Fe_{87}Pt_{13}-Al_2O_3$ composite films were fabricated by aluminothermy. We demonstrate that the RMA value in the $Fe_{87}Pt_{13}-Al_2O_3$ composite films exceeds that in the $Fe_{87}Pt_{13}$ samples by more than an order of magnitude.

2. EXPERIMENTAL

In this work, granular samples were prepared using the technique proposed in 1893 by Prof. G. Goldschmidt for reduction of metal oxides using aluminum powders in the highly exothermic reactions (aluminothermy) [23]. The $Fe_{87}Pt_{13}-Al_2O_3$ composite films were synthesized using chemical phase transformations consisting of several stages.

In the initial stage, Pt/Fe bilayers were formed by sequential thermal deposition (by electron bombardment of crucibles with Pt and Fe) onto single-crystal MgO(001) substrates in working vacuum with a residual pressure of over 10^{-6} Torr. The initial bilayer had the elemental composition Fe/Pt = 87/13 at % and a total thickness of ~200 nm. The Fe and Pt layers were deposited at temperatures of 220 and 280°C, respectively, at which the Fe(001) and Pt(001) layer grew epitaxially on the MgO(001) surface without solid-state reaction between them. The initial Pt(001)/Fe(001)/MgO(001) structure was sequentially annealed at temperatures from 300 to 550°C with a step of 50°C and exposure for 90 min in vacuum at a residual pressure of 10^{-6} Torr. X-ray and magnetic measurements were performed after each annealing step.

In the second stage, the synthesized $Fe_{87}Pt_{13}$ film was oxidized in air at 550°C until the sample magnetization completely vanished. The initial sample was formed by deposition of the aluminum layer onto the oxidized $Fe_{87}Pt_{13}$ sample surface in vacuum at a residual pressure of 10^{-6} Torr. The obtained structure was sequentially annealed at temperatures from 450 to 850°C with a step of 50°C and exposure for 90 min in vacuum at a residual pressure of 10^{-6} Torr.

The forming phases were identified by X-ray diffraction (XRD) on a DRON-4-07 diffractometer (CuK_α radiation, $\theta-2\theta$ geometry). The measurements of saturation magnetization M_S, magnetocrystalline anisotropy K_1 of the Fe(001) films, four-fold anisotropy K_4, and uniaxial anisotropy constant K_0 and iden-

tification of the rotational anisotropy upon variation in the torque curves were performed on a torque magnetometer with a maximum magnetic field of ~18 kOe. The in-plane torques $L_\parallel(\varphi)$ are given per unit volume.

Specimens for transmission electron microscopy (TEM) were prepared by the cross-sectional technique using a FIB, Hitachi FB2100 focused ion beam system. Electron microscopy investigations were carried out on a Hitachi HT7700 transmission electron microscope (TEM, 100 kV, W source) equipped with a scanning TEM system with an electron probe 30 nm in diameter and a Bruker Nano Xflash GT/60 energy-dispersive X-ray spectrometer. Chemical composition was determined on a Nano Bruker Quantax 70 device. All measurements were performed at room temperature. The special features of solid-state reactions in the $Al/(Pt + Fe_2O_3)$ system were examined by measuring the temperature dependence of the film resistivity by a four-probe method using pressed contacts in vacuum at a residual pressure of 10^{-6} Torr and a heating rate of ~5°C/min.

3. RESULTS AND DISCUSSION

3.1. Solid-State Synthesis and Magnetic Properties of the $Fe_{87}Pt_{13}$ film.

The cross section of the initial Fe/Pt sample presented in Fig. 1 reveals a bilayer structure consisting of the homogeneous Pt upper layer and the Fe lower layer with the column structure. X-ray diffraction spectra of the initial Fe/Pt bilayer samples contained a strong Fe(200) reflection indicative of the epitaxial growth of Fe(001) on the MgO(001) surface (Fig. 2a). The measured torque curves showed that the initial Pt(001)/Fe(001) samples were characterized by the four-fold anisotropy K_4 determined by the first crystallographic anisotropy constant $K_1^{Fe} = (5.0-5.1) \times 10^{-4}$ J/m^3 of the Fe(001) layer. This value agrees well with the K_1^{Fe} value for bulk Fe and Fe(001)/MgO(001) epitaxial films fabricated by different techniques [24]. The easy axes directions in the Fe layer coincide with the [110] and [1$\bar{1}$0] MgO(001) directions. This points out the existence of the orientational relationship [110](001)Fe ∥ [100](001) MgO typical of the Fe(001) films deposited onto MgO(001) by other methods. The above-mentioned facts are indicative of the high quality of the single-crystal Fe(001) films.

The single-crystal Pt(001)/Fe(001) bilayers were formed by depositing a platinum layer onto the Fe(001) layer at a substrate temperature of ~280°C, which provided the epitaxial growth of Pt(001) on the Fe(001) layer (Fig. 2a). Annealing at temperatures of up to 400°C did not change the X-ray diffraction patterns and four-fold anisotropy constants, which indicates the absence of intermixing and formation of compounds in the initial Pt(001)/Fe(001) bilayers. Annealing at 500°C facilitates the occurrence of an
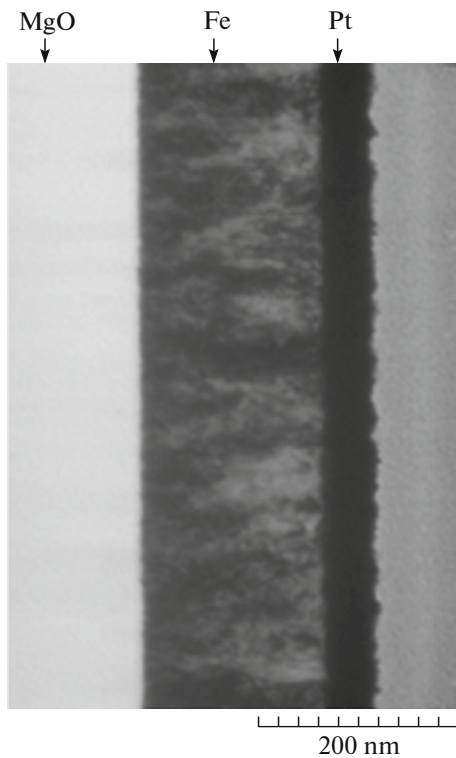
Fig. 1. Cross section of the initial Fe_{87}/Pt_{13} bilayer sample.

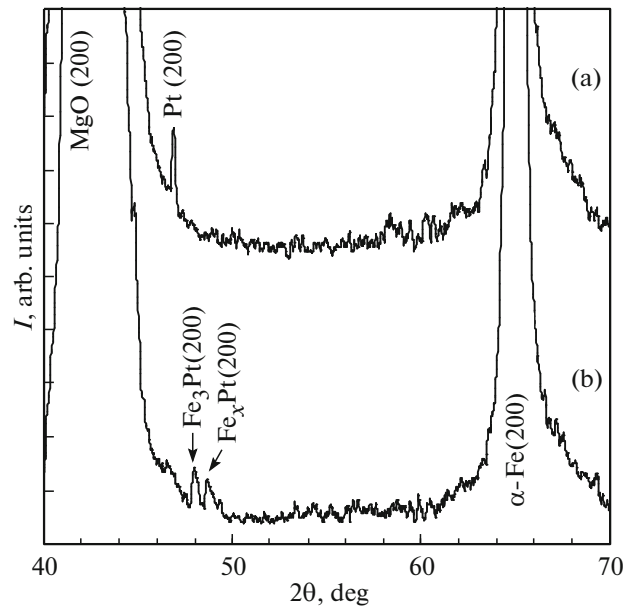**Fig. 2.** X-ray diffraction spectra of (a) the initial $Fe_{87}Pt_{13}$ bilayer sample and (b) $Fe_{87}Pt_{13}$ bilayer sample after annealing at $T = 500°C$.

intermediate layer consisting of the cubic ordered $L1_2$–Fe_3Pt and nonstoichiometric tetragonal $L1_0$–FePt phases at the Pt(001)/Fe(001) interface (Fig. 2b). Therefore, after annealing at 500°C, the samples had the Pt(001)/(Fe$_3$Pt + FePt)/Fe(001) structure. The in-plane torque curves show that the Pt(001)/(Fe$_3$Pt + FePt)/Fe(001) films are characterized by a special anisotropy type called the rotational magnetic anisotropy (RMA) (Fig. 3). The essence of this anisotropy is that the easy axis EA_0 initially aligned arbitrarily in the film plane rotates along with the magnetic field H by angle φ and sets in another position, EA_φ, lagging behind the magnetic field direction by angle α (Fig. 3a). The RMA can be characterized by the torque shift $\pm L_{rot}$ upon rotation of the magnetic field clockwise (+) and counterclockwise (−) (Fig. 3b) [18]. The torque curves retain, along with the RMA, the four-fold anisotropy K_4 (Figs. 3b and 3c). The RMA constant is $(4 \pm 0.5) \times 10^4$ erg/cm^3 and four-fold crystallographic anisotropy $K_4 = (2.5 \pm 0.5) \times 10^5$ erg/cm^3, which contains the contributions of Fe$_3$Pt(001), FePt(001), and Fe(001)0 grains.

According to the measured torque curves for the samples annealed at 550°C, the magnetic-field-induced RMA vanishes and the four-fold anisotropy weakens (Fig. 3d). The X-ray measurements of the Pt(001)/(Fe$_3$Pt + FePt)/Fe(001) sample above 500°C revealed the further solid-state reaction between the

Pt(001), Fe$_3$Pt(001) + FePt(001), and Fe(001) layers and the preferred formation of the disordered Fe$_3$Pt cubic phase, which reduces the four-fold anisotropy constant $K_4 < (5 \pm 0.5) \times 10^3$ erg/cm^3 and leads to the disappearance of the RMA. Presumably, the absence of the RMA in the samples synthesized in the temperature range of ~400–500°C originates from the formation of the mixture of $L1_2$ and $L1_0$ phases, which transforms to the magnetically soft Fe$_3$Pt/Fe(001) bilayer upon heat treatment at temperatures above this range.

3.2. Solid-State Synthesis and Magnetic Properties of the $Fe_{87}Pt_{13}$–Al_2O_3 film.

The $Fe_{87}Pt_{13}$–Al_2O_3 composite films were formed as follows. The initial Fe$_3$Pt/Fe(001) structure was oxidized in air until the magnetization completely vanished, indicating the formation of nonmagnetic iron oxides. After oxidation, the reaction products yielded the only diffraction reflection, (200)Pt, and peaks from polycrystalline α-Fe$_2$O$_3$ grains (X-ray diffraction patterns is not presented here). It means that the oxidized samples were composed from two phases: iron oxide α-Fe$_2$O$_3$ and single-crystal platinum grains. The obtained film composite Pt + Fe$_2$O$_3$ was coated with an Al layer with a thickness corresponding approximately to the 1Al : 1Fe atomic composition. To determine the characteristic reaction temperatures, the obtained Al/(Pt + Fe$_2$O$_3$) film systems were heated from 50 to 550°C in vacuum at a residual pressure of
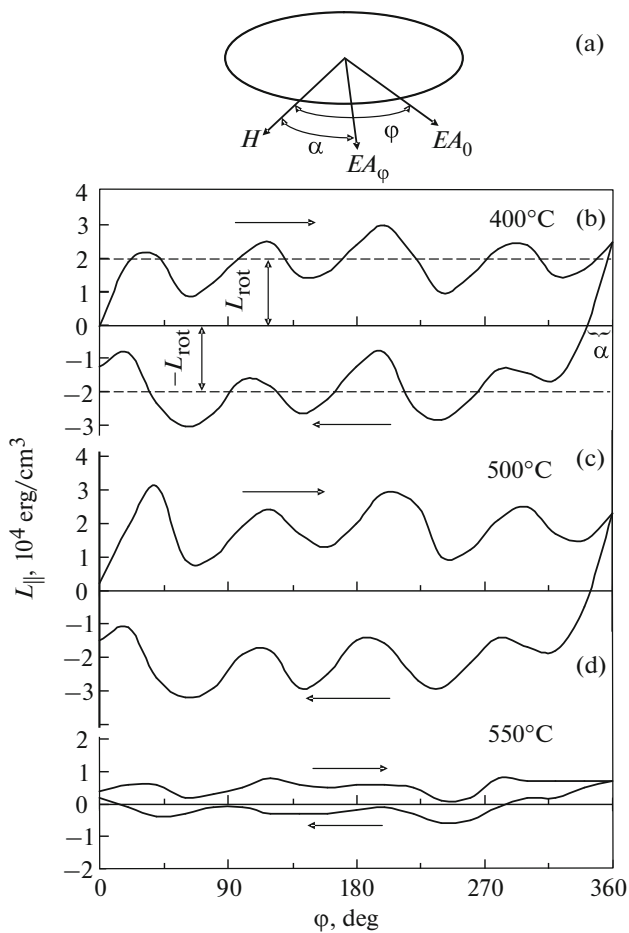
Fig. 3. (a) Schematic and (b) $L_{\parallel}(\varphi)$ torque curves for the film samples annealed at (b) 400°C, (c) 500°C, and (d) 550°C upon in-plane forward and backward rotation of the magnetic field $H = 10$ kOe by 360°.

Fig. 4. Temperature dependence of the resistance $R(T)$ in the Al/Pt + Fe$_2$O$_3$ film upon heating to 500°C and subsequent cooling to room temperature.

10^{-6} Torr with subsequent cooling to room temperature. Figure 4 shows the temperature dependence of the electrical resistance $R(T)$, which allows us to determine initiation temperatures of the chemical reactions in this system. It can be seen that the resistance is of the metal type up to ~430°C (inset in Fig. 4), which is determined by the upper aluminum layer and evidences for the absence of layer intermixing. At higher temperatures, a feature arises in the $R(T)$ dependence; specifically, R slightly increases upon temperature variation in the range of 430–525°C, which implies that the layer start mixing. At $T \sim 525$–530°C, the electrical resistance of the film sharply grows, which speaks about the beginning of the Goldschmidt thermite solid-state reaction $2Al + Fe_2O_3 = 2Fe + Al_2O_3$ occurring with the iron reduction and formation of the Al_2O_3 insulating matrix. Upon cooling, the $R(T)$ dependence becomes complex and now includes the semiconductor and metal portions. The electrical resistance increased by two orders of magnitude, 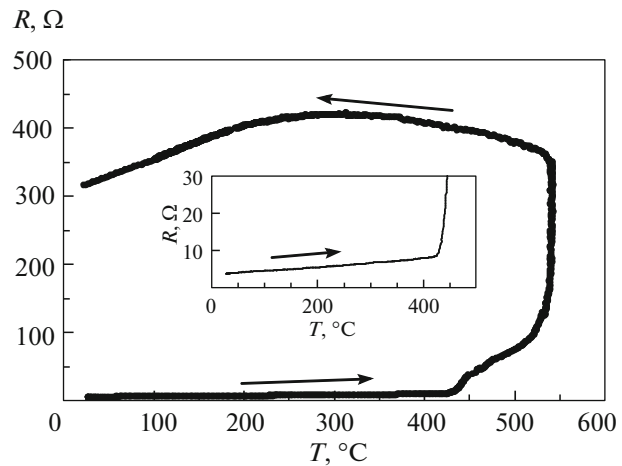totally due to the effect of the composite structure of the obtained films and the presence of the Al_2O_3 dielectric component. The electrical resistances measured at different heating temperatures are consistent with the XRD and magnetic structural data.

Since the reaction starts above 430°C, the obtained $Al/(Pt + Fe_2O_3)$ film system was annealed at temperatures from 450 to 850°C in vacuum at a residual pressure of 10^{-6} Torr. The measured torque curves show that upon annealing in the temperature range of 450–500°C, there is the RMA with a constant of no higher than $L_{rot} = 3.5 \times 10^4$ erg/cm^3 (Fig. 5a). The RMA constant increases by almost an order of magnitude ($\pm L_{rot} = 3.8 \times 10^5$ erg/cm^3) after annealing above 650°C and does not vanish up to 850°C (Figs. 5c and 5d). In this temperature range, the torque curves have a large unidirectional component with $K_0\sin\varphi$ ($K_0 = 3.4 \times 10^5$ erg/cm^3) typical of exchange-coupled structures with the uniaxial anisotropy (Figs. 5c and 5d).

In our opinion, the growth of constant L_{rot} and the occurrence of the uniaxial anisotropy are related to the structural transformations in $Al/(Pt + Fe_2O_3)$ samples with an increase in the annealing temperature from 450 to 850°C. According to the X-ray diffraction data shown in Fig. 6, the $L1_0$–FePt phase forms in the samples synthesized at an annealing temperature of 550°C. This suggests the following scenario of the $L1_0$ phase synthesis, which starts with iron reduction in the course of the classical Goldschmidt thermite reaction. The reduced iron reacts with platinum with the formation of $L1_0$–FePt grains. As the annealing temperature increases, the magnetization grows due to an increase in the $L1_0$-phase volume and partial chemical transformation α-Fe$_2$O$_3$ → Fe$_3$O$_4$. The further growth of the annealing temperature to 850°C also induces the
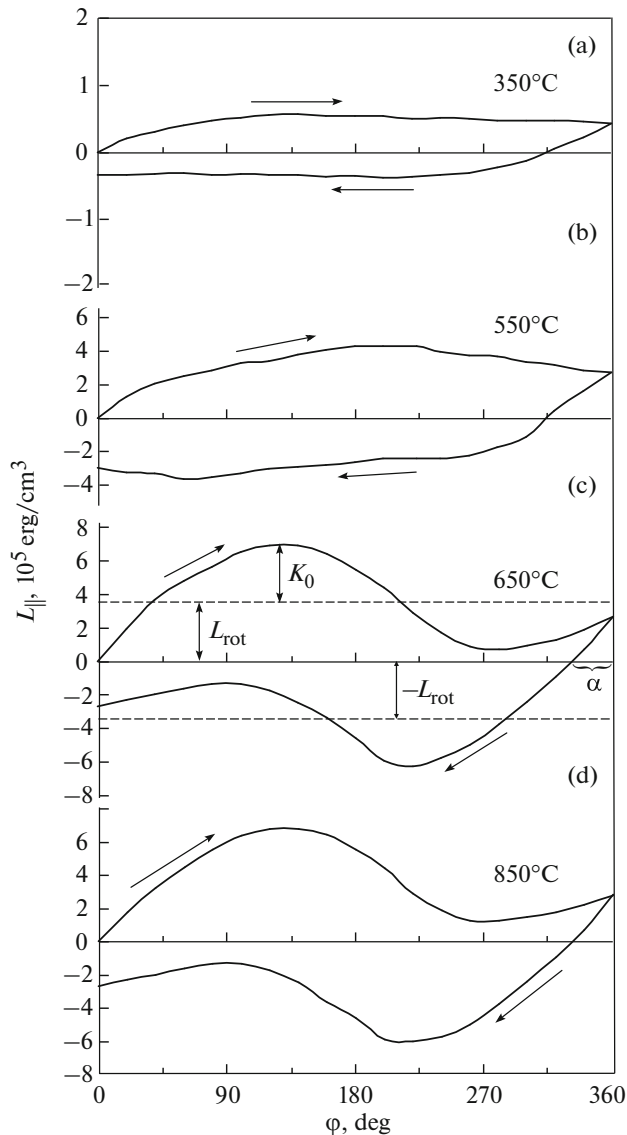
Fig. 5. $L_{\parallel}(\varphi)$ torque curves of the $Fe_{87}Pt_{13}-Al_2O_3$ film samples annealed at (a) 450°C, (b) 550°C, (c) 650°C, and (d) 850°C upon in-plane forward and backward rotation of the magnetic field $H = 10$ kOe by 360°.

chemical reaction $Fe_3O_4 \rightarrow \gamma\text{-}Fe_2O_3$. Along with iron oxides, the synthesized sample contains aluminum and manganese oxides (Fig. 6b).

The phase formation in the $Fe_{87}Pt_{13}-Al_2O_3$ film annealed at 850°C is confirmed by the electron microscopy investigations of the film cross section (Fig. 7). Microphotographs with the elemental distribution over film thickness, which was determined using an energy-dispersive X-ray spectrometer, show a very complex structure consisting approximately of three parts (Fig. 7). The first part is the highly anisotropic $L1_0-FePt$ film located near the substrate, the second part is the magnetic iron oxide $\gamma\text{-}Fe_2O_3$, and
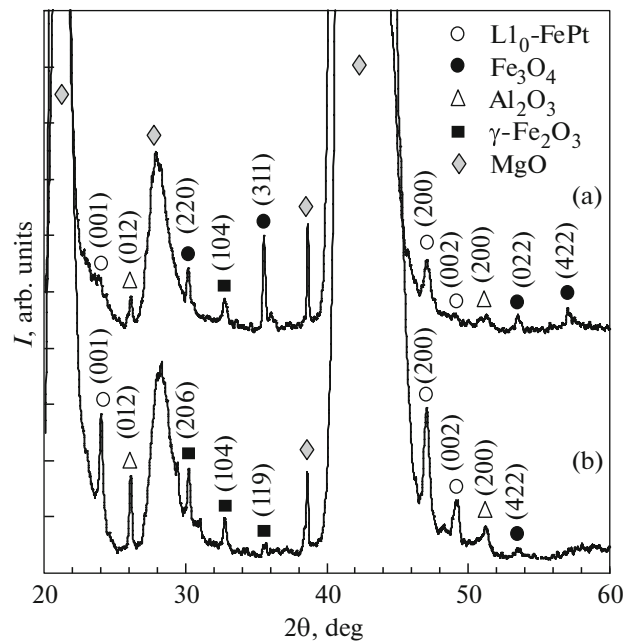

Fig. 6. X-ray diffraction spectra of the $Fe_{87}Pt_{13}-Al_2O_3$ films annealed at (a) 550°C and (b) 850°C.

the third part is the Al_2O_3 surface layer. The iron oxide is partially distributed in the FePt phase and the aluminum oxide, over the entire film thickness. The established distribution of structural parts in the cross section of the $Fe_{87}Pt_{13}-Al_2O_3$ composite film is consistent with the XRD data (Fig. 6).

Analysis of the X-ray and magnetic measurement data allows us to conclude that the RMA in the synthesized $Fe_{87}Pt_{13}-Al_2O_3$ composite samples originates from the exchange coupling between the ferromagnetic $L1_0-FePt$ phase and ferrimagnetic iron oxides $Fe_3O_4 + \gamma\text{-}Fe_2O_3$. The exchange-coupled model is often used to explain the nature of RMA in films [18].

There exist numerous literature data on the RMA in film systems and on the mechanisms responsible for its occurrence [18, 25–29]. In different works, the RMA is assumed to be caused by domain structure rearrangement, exchange coupling, martensitic transformations, controlled magnetostriction, etc. However, there still has been a lack of convincing models that could explain this effect [18]. The nature of RMA observed in the $Fe_{87}Pt_{13}$ and $Fe_{87}Pt_{13}-Al_2O_3$ film structures synthesized in this work remains unclear, but the RMA always occurs with the formation of the $L1_{10}-FePt$ phase and always vanishes with its disappearance. This makes us attribute the nature of RMA to the exchange coupling between the $L1_0-FePt$ and $L1_2-Fe_3Pt$ phases in $Fe_{87}Pt_{13}$ and iron oxides in the $Fe_{87}Pt_{13}-Al_2O_3$ samples.
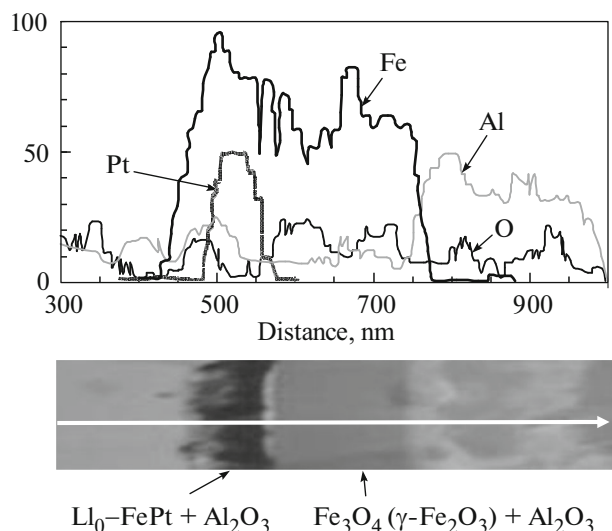
Fig. 7. Cross section and elemental composition of the $Fe_{87}Pt_{13}$–Al_2O_3 composite film annealed at 850°C.

4. CONCLUSIONS

It was shown that annealing of the Fe(001)/Pt(001) bilayer film deposited onto the single-crystal MgO substrate with the atomic elemental ratio of 83 : 17 at temperatures starting from 350°C leads to the formation of magnetic phases characterized by the in-plane rotational magnetic anisotropy, which completely vanishes upon annealing at 500°C. Study of the $Fe_{87}Pt_{13}$–Al_2O_3 composite structure formed from the Fe/Pt bilayer sample with the same concentration ratio by aluminothermy and annealed at 550°C showed the presence of RMA, which increases by more than order of magnitude upon annealing at 550°C and remains after heat treatment at temperatures of up to 850°C. The occurrence of RMA in $Fe_{87}Pt_{13}$–Al_2O_3 was attributed to the exchange coupling of the two magnetic phases: ferromagnetic $L1_{10}$–FePt phase and ferrimagnetic iron oxides.

ACKNOWLEDGMENTS

REFERENCES

1. A. Kohn, N. Tal, A. Elkayam, A. Kovàcs, D. Li, S. Wang, S. Ghannadzadeh, T. Hesjedal, and R. C. C. Ward, Appl. Phys. Lett. **102**, 062403 (2013).

2. Fu-Te Yuan, A. C. Sun, J.-K. Mei, W. M. Liao, J.-H. Hsu, and H. Y. Lee, J. Appl. Phys. **109**, 07B743 (2011).

3. C. Feng, X. Li, M. Yang, K. Gong, Y. Zhu, Q. Zhan, L. Sun, B. Li, Y. Jiang, and G. Yu, Appl. Phys. Lett. **102**, 022411 (2013).

4. Z. Lu, J. Guo, Z. Gan, Y. Liu, R. Xiong, and G. J. Mankey, J. Appl. Phys. **113**, 073912 (2013).

5. G. R. Trichy, D. Chakraborti, J. Narayan, and H. Zhou, J. Appl. Phys. **102**, 033901 (2007).

6. A. Kovàcs, K. Sato, and Y. Hirotsu, J. Appl. Phys. **102**, 123512 (2007).

7. K. F. Dong, H. H. Li, and J. S. Chen, J. Appl. Phys. **113**, 233904 (2013).

8. H. Bernas, J.-Ph. Attané, K.-H. Heinig, D. Halley, D. Ravelosona, A. Marty, P. Auric, C. Chappert, and Y. Samson, Phys. Rev. Lett. **91**, 077203 (2003).

9. F. Tournus, K. Sato, T. Epicier, T. J. Konno, and V. Dupuis, Phys. Rev. Lett. **110**, 055501 (2013).

10. H. Ho, E. Yang, D. E. Laughlin, and J.-G. Zhu, Appl. Phys. Lett. **102**, 112411 (2013).

11. C. W. White, S. P. Withrow, K. D. Sorge, A. Meldrum, J. D. Budai, J. R. Thompson, and L. A. Boatner, J. Appl. Phys. **93**, 5656 (2003).

12. D. A. Gilbert, L.-W. Wang, T. J. Klemmer, J.-U. Thiele, C.-H. Lai, and K. Liu, Appl. Phys. Lett. **102**, 132406 (2013).

13. S. Pisana, O. Mosendz, G. J. Parker, J. W. Reiner, T. S. Santos, A. T. McCallum, H. J. Richter, and D. Weller, J. Appl. Phys. **113**, 043910 (2013).

14. Y. Wang, X. Zhang, Y. Liu, S. Lv, Y. Jiang, Y. Zhang, H. Liu, Y. Liu, and J. Yang, J. Alloys Compd. **582**, 511 (2014).

15. L. N. Yu, L. Y. Lu, Z. D. Xu, X. G. Xu, J. Miao, and Y. Jiang, Mater. Lett. **86**, 142 (2012).

16. D. Weller, O. Mosendz, G. Parker, S. Pisana, and T. S. Santos, Phys. Status Solidi A **210**, 1245 (2013).

17. M. A. I. Nahid and T. Suzuki, J. Appl. Phys. **97**, 10K307 (2005).

18. V. G. Myagkov, V. S. Zhigalov, B. A. Belyaev, L. E. Bykova, L. A. Solovyov, and G. N. Bondarenko, J. Magn. Magn. Mater. **324**, 1571 (2012).

19. V. G. Myagkov, L. E. Bykova, G. N. Bondarenko, V. S. Zhigalov, A. I. Pol'skii, and F. V. Myagkov, JETP Lett. **71** (5), 183 (2000).

20. V. Myagkov, O. Bayukov, Y. Mikhli, V. Zhigalov, L. Bykova, and G. Bondarenko, Philos. Mag. **94**, 2595 (2014).

21. V. G. Myagkov, V. S. Zhigalov, L. E. Bykova, L. A. Solov'ev, and G. N. Bondarenko, JETP Lett. **91** (9), 481 (2010).

22. S. M. Zharkov, E. T. Moiseenko, R. R. Altunin, N. S. Nikolaeva, V. S. Zhigalov, and V. G. Myagkov, JETP Lett. **99** (7), 405 (2014).

23. V. S. Zhigalov, V. G. Myagkov, V. A. Cemyachkov, G. N. Bondarenko, and I. V. Nemtsev, Solid State Phenom. **215**, 218 (2014).

24. K. Noda, M. Higuchi, Y. Komaki, T. Tanaka, Y. Nozaki, and K. Matsuyama, J. Phys.: Conf. Ser. **266**, 012014 (2011).

25. M. Barturen, M. Sacchi, M. Eddrieff, J. Milano, S. Bustingorry, H. Popescu, N. Jaouen, F. Sirotti, and M. Marangolo, Eur. Phys. J. B **86**, 191 (2013).

26. H. Fujiwara, Y. Sugita, and N. Saito, Appl. Phys. Lett. **4**, 199 (1964).

27. J. M. Lommel and C. D. Graham, Jr., J. Appl. Phys. **33**, 1160 (1962).

28. E. S. Leva, R. C. Valente, F. M. Tabares, M. V. Mansilla, S. Roshdestwensky, and A. Butera, Phys. Rev. B: Condens. Matter **82**, 144410 (2010).

29. R. F. Soohoo, *Magnetic Thin Films* (Harper and Row, New York, 1965; Mir, Moscow, 1967).

Translated by E. Bondareva